Summer 2018

Analysis of Fiber Network Architecture in Blood Vessels and Blood Clots

Dustin Michael Nguyen
San Jose State University

ANALYSIS OF FIBER NETWORK ARCHITECTURE IN BLOOD VESSELS AND BLOOD CLOTS

A Thesis

Presented to

The Faculty of the Department of Biomedical, Chemical and Materials Engineering

San José State University

In Partial Fulfillment

of the Requirements for the Degree

Master of Science

by

Dustin Nguyen

August 2018

The Designated Thesis Committee Approves the Thesis Titled

ANALYSIS OF FIBER NETWORK ARCHITECTURE IN BLOOD VESSELS AND BLOOD CLOTS

By

Dustin Nguyen

APPROVED FOR THE DEPARTMENT OF BIOMEDICAL, CHEMICAL, AND MATERIALS ENGINEERING

SAN JOSÉ STATE UNIVERSITY

August 2018

Anand Ramasubramanian, Ph.D.	Department of Biochemical, Chemical, and Materials Engineering
Amit Saha, Ph. D.	Department of Biochemical, Chemical, and Materials Engineering
Markus Wagenhaeuser, M.D.	Resident Vascular Surgery, Department of Vascular and Endovascular Surgery, Heinrich Heine University
Matthew Leineweber, Ph. D.	Department of Biochemical, Chemical, and Materials Engineering

ABSTRACT

ANALYSIS OF FIBER NETWORK ARCHITECTURE IN BLOOD VESSELS AND BLOOD CLOTS

by Dustin Nguyen

Fibrous networks, including collagen and fibrin, provide strength and support, and are critical for maintaining homeostasis. In this study, we have developed algorithms to define the structural properties of collagen and fibrin networks from microscopic images of these networks in abdominal aortic aneurysms (AAA) and blood clots, respectively. AAA is a biomechanical disease characterized by significant changes in the structure and strength of the arterial wall due to differential changes in the composition of fibrillar collagen in adventitial and medial layers. Using bright-field and polarized microscopic images of histological sections of mouse aorta stained with Picrosirius red (PSR) stain, we developed MATLAB code to locally quantify collagen content within the vessel wall. The method was benchmarked against manual quantification, and the superiority of the automated analysis was established by statistical analyses of accuracy and reproducibility. Fibrin networks form the structural and functional basis of blood clots. We developed an algorithm using a combination of ImageJ plugins and a custom MATLAB code to analyze the ultrastructure of blood clots from the scanning electron microscopic images of fibrin networks. This morphometric profile was used to correlate clot structure to mechanics, which has implications for our understanding of hemostasis and thrombosis.

ACKNOWLEDGEMENTS

I would like to express gratitude towards Dr. Anand Ramasubramanian for taking me into his lab and providing the resources and guidance that allowed this endeavor to be completed. Without the time he invested in me, this paper would not be possible.

Much gratitude is also due for my committee members, Dr. Amit Saha, Dr. Markus Wagenhaeuser, and Dr. Matthew Leineweber. The support and guidance they offered was invaluable. They gave me the jumpstart to begin my progression of this thesis.

To my family and loved ones, I am especially grateful for all of you. Thank you for keeping my heart in good spirits and keeping me motivated to keep achieving. I truly am who I am now thanks to you all.

This work is dedicated to the memories of Amaya Sydney Lumpkins and Tam Thi Tran.

TABLE OF CONTENTS

LIST OF TABLES

LIST OF FIGURES

CHAPTER ONE: INTRODUCTION

Soft tissue, such as blood vessels and muscle, contains an extracellular matrix (ECM) comprised of proteins and proteoglycans. The mechanical properties of the ECM are determined by the underlying networks of proteins, predominantly collagen, and, depending on the tissue, elastin, fibronectin or laminin. Collagen is also an important constituent of synthetic ECM analogs for tissue engineering applications. Fibrin is also key to life, as it forms the structural and functional basis of blood clots. The biocompatibility and ECM-like properties make fibrin gels a desirable candidate for tissue engineering applications. Both collagen and fibrin are hydrogels with highly interwoven networks of fibers. The mechanical properties of collagen and fibrin matrices are dependent not only the collagen and fibrin content, but also on network architecture. Thus, understanding the properties of the fibrous network on the microscale can be critical for characterizing the behavior of different tissue in health and disease.

1.1 The Importance of Collagen

Collagen is a key structural component in the ECM of soft tissue and accounts for approximately one third of the protein in the human body [1]. Collagen and elastin are components of the blood vessel wall that contribute to the strength of the vessel wall, and the quantity and structure of the collagen are primarily what define the mechanical properties of the vessel wall, including abdominal aortic aneurysms (AAAs).

The arterial wall is comprised of three layers, the intima, media, and adventitia. The intima is the innermost layer of the three and is very fine, colorless, and transparent. It is

comprised of endothelial cells, connective tissue, and some elastic fibers. The media is the middle layer and it is the most important layer when analyzing the mechanical properties of the artery [5]. It is composed of collagen bundles and elastin fibers and sheets. The adventitia is the outermost layer and it contains elastin fibers and denser collagen fibers. Therefore, the quantities of collagen within a vessel wall are determined by quantifying the amount of collagen within the media and adventitia, as can be seen in Figure 1.

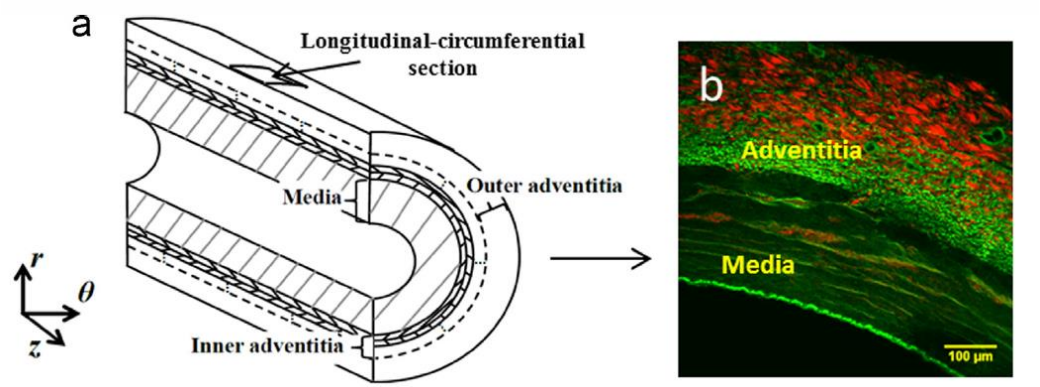

Figure 1. (a) Schematic of an artery layer structure (b) Second harmonic generation microscopy and two-photon-excited fluorescence microscopy image of an arterial cross-section. Green represents the elastin fibers and red represents the collagen (reprinted with permission from Elsevier) [5].

When the elastin in the media of the vessel wall is depleted, the collagen in the adventitia is primarily responsible for the resistance of the vessel wall to rupturing and the degradation and reorganization of collagen is ultimately the reason for rupture [3]. AAAs are dilations of the infrarenal aorta, including the renal ostia (intrarenal and suprarenal aorta). AAA formation is associated with weakening of the structural components in the vessel wall. The ECM of the AAA also contains smooth muscle tissue,

but it has been shown that the smooth muscle tissue does not significantly affect the static mechanical properties of a mature aorta [2]. Aneurysmal tissue shows a decreased concentration of elastin and the depletion of elastin happens early in the formation of the aneurysm [3, 4]. Histological samples of AAA tissue show a decreased concentration of elastin and collagen when compared with a healthy vessel wall [6]. The degradation of elastin during the growth of the aneurysm is the earliest step in aneurysm formation. Once the aneurysm is formed, the collagen in the wall becomes the primary defense against rupturing. It has been seen in animal cells that new collagen can form in response to the aneurysm, which creates a catabolic environment for the collagen leading to rupture [7].

The extent of the dilation of AAA varies dependent on age, sex, and body weight. AAAs continue to expand over time and will rupture if the stress alongside the vessel wall overcomes the strength of the wall. Most AAAs will continue to present no symptoms until this rupturing occurs, which is fatal for 65% of patients [3]. The risk of rupturing increases as the dilation of the aorta increases. This risk is also increased by several factors such as genetic history, tobacco smoking, and chronic pulmonary disease. AAA treatment options start with monitoring the aneurysm regularly via ultrasound. If the AAA grows to greater than five centimeters or is growing at a rapid rate, surgery is recommended to remove the affected area of the aorta and replace the damaged section with a graft [3].

Tobacco smoking has been closely linked to aneurysm development, and it has been demonstrated that the occurrence of AAA in tobacco smokers is more than four times that of non-smokers [1]. It has been suggested that tobacco smoking leads to the interference of the enzymes responsible for collagen metabolism in the arterial wall [5–7]. However, the biological mechanisms linking smoking and aneurysm growth remain unknown [1, 5]. With the advent of electronic cigarettes and vaporizers, the effect of nicotine without tobacco on aneurysm formation and growth must be studied.

It is common practice to quantify the collagen content in AAA by taking histological samples, pulverizing them in liquid nitrogen, and assaying for collagen content, typically by zymography. However, this process only accounts for the overall quantity of collagen found in the vascular wall and does not allow for the analysis of local quantities of collagen throughout the vessel wall. This method is also unable to determine the organization of the fibers. Analyzing the localized variation and orientation of the fiber network will allow for further understanding of vessel wall strength and will also show changes in orientation when comparing healthy and treated tissue.

1.2 The Importance of Fibrin

Fibrin is a key component of hemostasis and must be structurally sound to form a stable clot that is able to endure the force of blood flow. If a blood vessel is damaged, fibrin is produced by catalyzing fibrinogen by thrombin, and fibrin is formed into a mesh that captures activated platelets and blood cells to form a clot [10]. Thrombin concentration is a critical factor in fibrin polymerization kinetics and a decrease in the

ratio of thrombin to fibrinogen leads to slower reaction kinetics and larger fiber diameters [11]. Abnormalities or weaknesses in the fibrin network can cause the clot to rupture or embolize, which can lead to stroke or the need for angioplasty. The structural mechanics of fibrin networks can be linked to the orientation properties of the network. The viscoelastic properties of fibrin are particularly sensitive to changes in the structure of the fibrin network. Understanding structural mechanics is important for predicting the likelihood of disease, such as venous vs. arterial thrombosis, and the clinical outcomes post-thrombectomy or surgical removal of clots.

1.3 Importance of Quantifying the Properties of Fibrous Network Structures

The structural mechanics of these fibrous network structures can be related to their microstructural properties, such as fiber density, branch density, and fiber orientation, as form defines function. It is known that the ultrastructure of the fibrin mesh can be altered by multiple factors such as thrombin concentration, pH, and calcium concentration [12]. Previously, an inverse relationship between thrombin concentration and total fiber length and fiber diameter was observed [13]. The temperature of the platelets has also been shown to have an effect on the observed strength of the fibrin network, with cold-induced plasma demonstrating increased cross-linking, induced by improved factor XIII binding to platelet surfaces [14]. Quantifying the microstructural properties using image analysis allows for correlations to be made between the microstructure and the structural mechanics of these soft tissue. The use of imaging software allows for the rapid

quantification of these fibrous networks and can be further accelerated using automated and semi-automated properties.

CHAPTER TWO: LITERATURE REVIEW

2.1 Collagen Quantification

As previously mentioned, the arterial wall is characterized by three layers, the intima, media, and adventitia. The mechanical properties of the blood vessel are largely determined by the structure and quantity of the collagen within the vessel walls. Numerous studies have been conducted to analyze the amount of collagen within various soft tissue in the pursuit of understanding the effects that disease regarding soft tissue.

Minion et al. used serial extraction techniques on aortic tissue to remove the proteins, calcium, and lipids [15]. An amino acid analysis was conducted on the extracted samples using a Beckman 6300 Amino Acid Analyzer to determine the amounts of hydroxyproline (HPro), desmosine (Des), and isodesmosine (ide). The amounts of desmosine and isodesmosine indicated the content of elastin-specific cross-links, which was directly proportional to the elastin content. The collagen content was determined in the same manner by using the content of hydroxyproline. Minion et al. determined that the amount of desmosine and isodesmosine relative to the total amount of protein would decrease as the aneurysm grew but the actual content of elastin increased as seen in Table 1 [15]. The collagen content increased much more than the elastin increased, indicating that the elastin concentration decreased due to dilution from an increase in other components within the ECM.

Table 1. Amino Acid Analyzer results of normal aorta (NL) and AAA

Sample Type	Protein	HPro	Des/ide
AAA	403 ± 116	14.1 ± 2.6	0.57 ± 0.07
NL	48 ± 8	2.9 ± 0.5	0.23 ± 0.03

Elastin and collagen content in AAA were determined by Carmo et al. using the same polyaminoacids as Minion et al., along with hydroxylysine as another marker to identify collagen content [16]. The collagen content was determined using colorimetric methods and gas chromatography. Carmo et al. determined that elastin and total protein content were reduced in AAA walls and the change in collagen content varied between studies. The collagen content decreased but the number of cross-links increased. Thus, Carmo et al. proposed that the mechanism to create new collagen is stunted while the old collagen continues to create cross-links.

Minion et al. and Carmo et al. were able to determine the overall collagen content in AAA tissue samples by using hydroxylysine and hydroxyproline as markers for collagen. However, these methods are not adequate for determining localized collagen content because the tissue samples are pulverized or hydrolyzed and evaporated. The layers of the AAA cannot be separated easily for separate analysis due to the friability of the layers.

2.2 Imaging Techniques

Rich et al. used imaging software, PSR, and polarized light to determine the collagen content in skin, myocardial tissue, and arterial tissue [17]. Collagen that is stained with PSR appears green, yellow, orange, or red under polarized light [18]. The color of the staining under polarized light has been used in some studies to differentiate between

different types of collagen, while other studies use the color to indicate the packing and thickness of the collagen fibers. Rich et al. defined the colors of interest in the images of PSR-stained tissue as red, orange, yellow, and green by desaturating the image and assigning ranges of hue to the colors. These color thresholds were then applied to five more images to ensure reproducibility using the same numerical values for hue. The darker portions of the polarized image are all interstitial space and non-collagen elements which were removed from the image. The types of collagen were quantified by taking the pixel count of one of the colors (i.e. orange or red) and comparing that value to total number of collagen pixels observed. Using these methods, the arterial adventitia was determined to be 89% collagen with a composition of 55% yellow, 25% orange, and 17% green [17]. The media comprised 54% collagen with a composition of 41% yellow, 8% orange, and 50% green.

Vogel et al. utilized different imaging software to determine the collagen content of PSR stained tissue utilizing fluorescence microscopy [19]. The techniques used for image subtraction are similar to the methods in the study done by Rich et al. but this analysis used a semi-automated algorithm. Vogel et al. used a combination of bright-field microscopy and fluorescent microscopy to determine which areas of the image contain live cells that are not of interest. Figure 2 demonstrates how the tolerance setting is a

large contributor to the observed amount of collagen and must be noted because it determines the detected area for the program to observe.

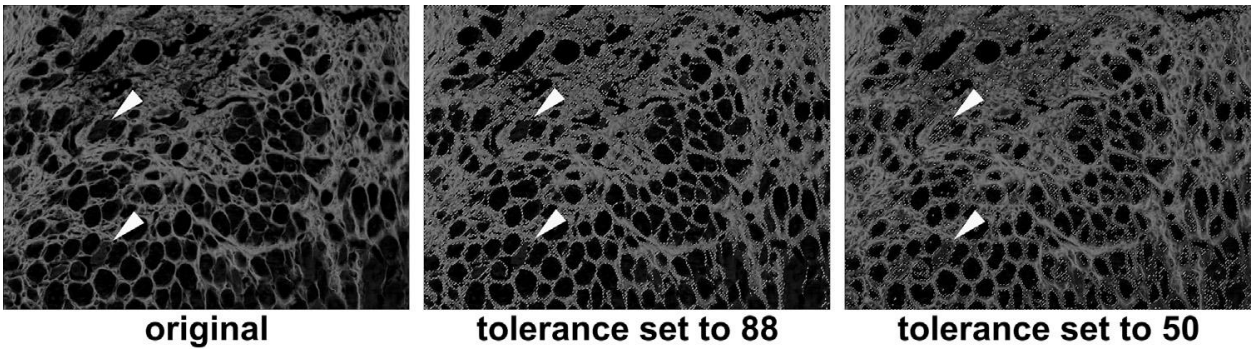

Figure 2. Effect of tolerance setting on automatic area detection [19].

A disadvantage of using polarized light in conjunction with PSR for collagen quantification is that if linear polarized light is used, some of the collagen that should appear stained will appear dark if it is aligned with the transmission axis of the polarized light filters. Rotating the platform can help mitigate this issue, but Lattouf et al. determined that the colors of the fibers can change by rotating the platform 90° as seen in Figure 3 [18]. Lattouf et al. states that the mechanisms of the interactions between collagen bundles and PSR cannot provide any evidence for specific interactions between collagen types.

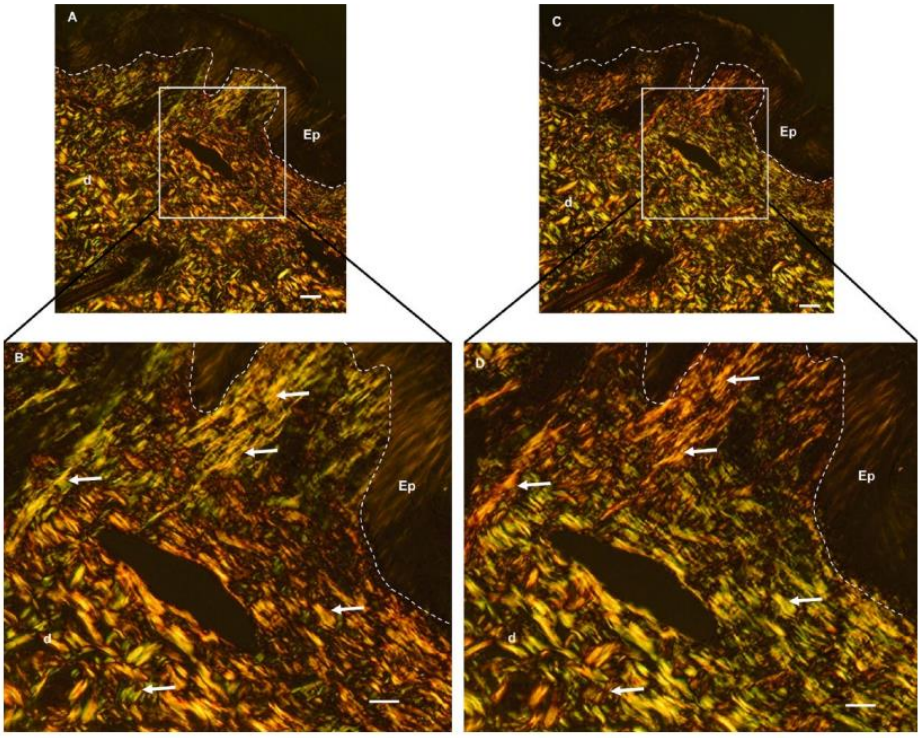

Figure 3. Skin section dyed with PSR (A) under polarized light microscopy. (C) is the same section after rotating the stage 90°. (B) and (D) are enlarged segments of (A) and (C), respectively (reprinted with permission from SAGE Publications) [18].

2.3 Fiber Orientation

There are different methods for measuring the orientation of a fiber network. Sander et al. utilized and compared three methods of measurement, Fourier transform method (FTM), mean intercept length (MIL), and line fraction deviation (LFD), to characterize the fiber orientation of images of simulated fiber networks [20]. The accuracy of the three methods was determined with respect to defining the principal direction and anisotropy index. It was ultimately determined that the FTM method provided the best accuracy and run time. The MIL had comparable accuracy to FTM but proved to be significantly

slower and LFD proved to be inadequate when compared to FTM and MIL. FTM was also determined to be a versatile measuring method because it can be optimized for an image to allow for improved accuracy and noise reduction. This provides a way to analyze high-resolution SEM images if the grayscale values were normalized.

Chen et al. determined the microstructural properties of collagen fibers by defining the orientation angle and waviness [21]. Multiphoton microscopy (MPM) images were analyzed by manually drawing center lines for each fiber and smoothed using B-spline interpolation in MATLAB. The orientation angle was then defined as the angle between the center-line and the direction of the line and the ratio of the arc-length to the total length of the fiber was defined as the waviness, as seen in Figure 4. The waviness varied between different layers of the wall but become uniform and straightened when put under high loads. The elastin fiber orientation was parallel with the collagen fibers and form a lattice like a net. This suggests that deformation in the wall is primarily due to the change of collagen content and orientation in animal models.

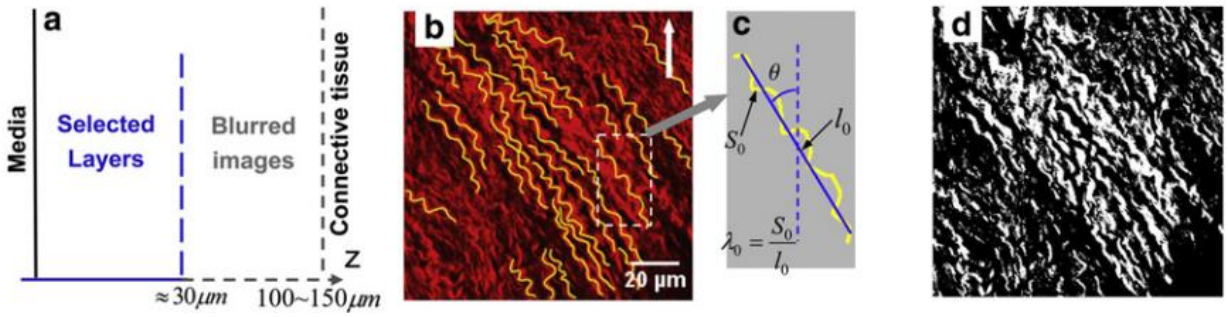

Figure 4. (a) Selected fiber layers of inner adventitia (b) Manually drawn center lines for fibers (c) Definition of orientation angle, θ, and waviness, λ_0 (d) Threshold of MPM image (reprinted with permission from Elsevier) [21].

Collagen is able to change its shape when under an applied load. Vader et al. developed an apparatus to analyze the effects of strain-induced alignment on collagen and observed that the reversibility of the collagen alignment after strain was dependent on the crosslinks in the collagen network [22]. The orientation of the fibers was determined using fluorescent beads within the collagen gel to create a grid to track the deformation of the gel at a microscale. Direct imaging of the fibers was used to display the statistical information for the orientation of the fibers, as seen in Figure 5.

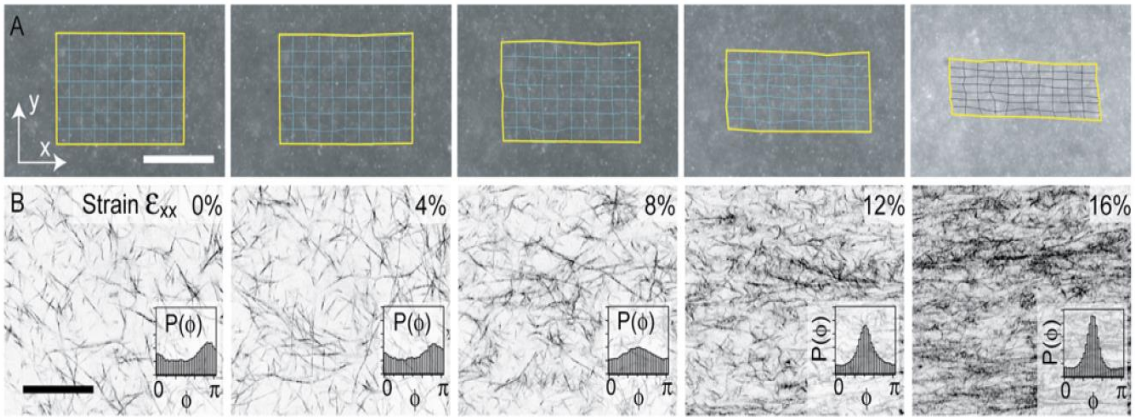

Figure 5. (A) Images of beads within collagen gel with grid to track the deformation (B) Direct imaging of the fibers with a histogram to denote variance in fiber orientation angle [22].

Other fiber networks, such as fibrin networks, have been analyzed using SEM images of the networks. D'Amore et al. developed an automated method using the image analysis toolbox in MATLAB to determine the density, spatial position and amount of fiber intersections [23]. This algorithm was also able to determine the fiber orientation angle distribution and diameter distribution. The images required pre-processing in MATLAB using three by three median filtering and histogram equalization to reduce the

noise and increase contrast, while not reducing the integrity of the edges. The grey levels of the image were then evened out by analyzing subdivisions of the image. The appropriate threshold for each subdivision was determined using the Otsu method [24]. This calculates the optimum thresholding as to define the foreground and background pixels while minimizing the intra-class variance. thin, smooth, and remove the pixels that were isolated and not part of the scaffold fibers. The image was further processed to highlight the edges and establish a skeleton of the fibers.

Fiber intersections were detected by evaluating circular coronas of pixels centered at each pixel in the image in 10° increments. The intensity values of these pixels were plotted versus the angle and it was determined that the number of peaks in the plot would determine the amount of fibers intersecting in the area around the analyzed pixel. If two or more peaks were observed, the pixel was considered to belong to an area with fiber intersections. The totality of the pixels within the areas with fiber intersections were used to create a new binary image. This image was then cleaned up further using the built-in image toolbox in MATLAB. The actual amount of fibers intersecting was determined using the center of mass of the intersection areas.

The determination of the fiber diameter must be done semi-automatically. The operator must manually establish a maximum fiber diameter to limit the length of segments analyzed perpendicular to the fiber. Fiber edges were detected using the intensity levels of the pixels along the segment direction. Using the levels of grey

intensity along the segment length, the representative fiber length was determined by using five points along the intensity curves, as seen in Figure 6.

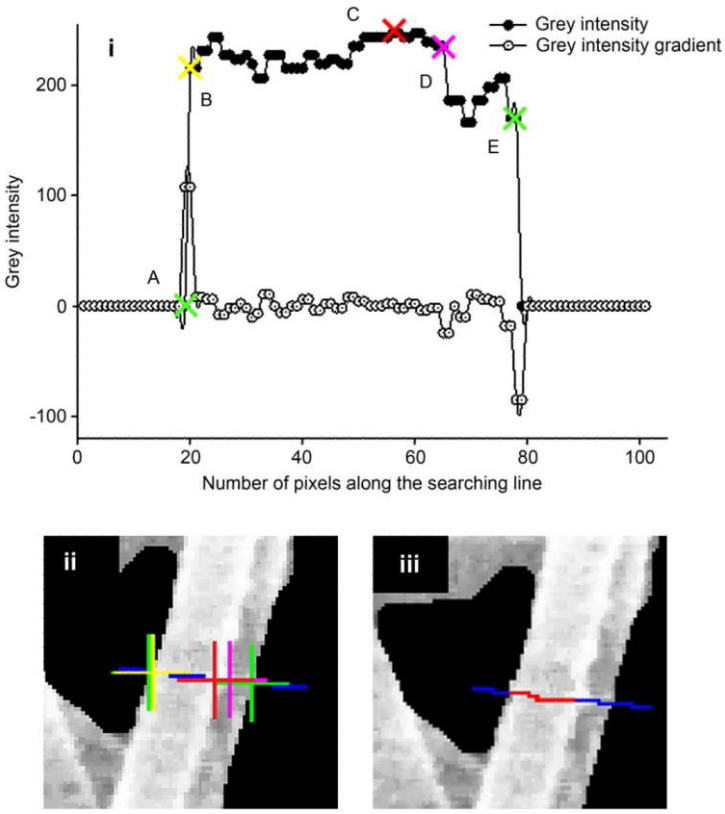

Figure 6. Fiber diameter detection using five points from the detected grey levels and the intensity gradient (reprinted with permission from Elsevier) [23].

Leonidakis et al. used MATLAB to determine the characteristics of fibrin gels using fluorescent confocal microscopy [12]. Figure 7 outlines the fiber analysis algorithm used. The properties that were quantified were total fiber length, hydrogel fiber density, fiber volume fraction, branch density, and fiber connectivity. This data was used to correlate the microstructure of the gels and the solubility of dextran through the fibrin gel.

There are currently some MATLAB applications that were developed to either automatically or semi-automatically determine the characteristics of fiber networks. An application developed by Persson et al., called GTFiber, utilizes a five-step process to produce an orientation map, where each fiber is thinned to the width of a single pixel and an orientation is determined for each pixel [25]. The steps for treating the image are described as: anisotropic diffusion filtering, top hot filtering, thresholding, skeletonization, and orientation mapping. Persson et al. demonstrated the use of the application on atomic force microscopy (AFM) images, as seen in Figure 8. The results of the image treatment process are dependent on user defined parameters which affect the degree of processing is done on the original image. Although GTFiber was developed in MATLAB and can be run as a script in MATLAB, there is also a standalone application for GTFiber that is available for Windows and Mac OS.

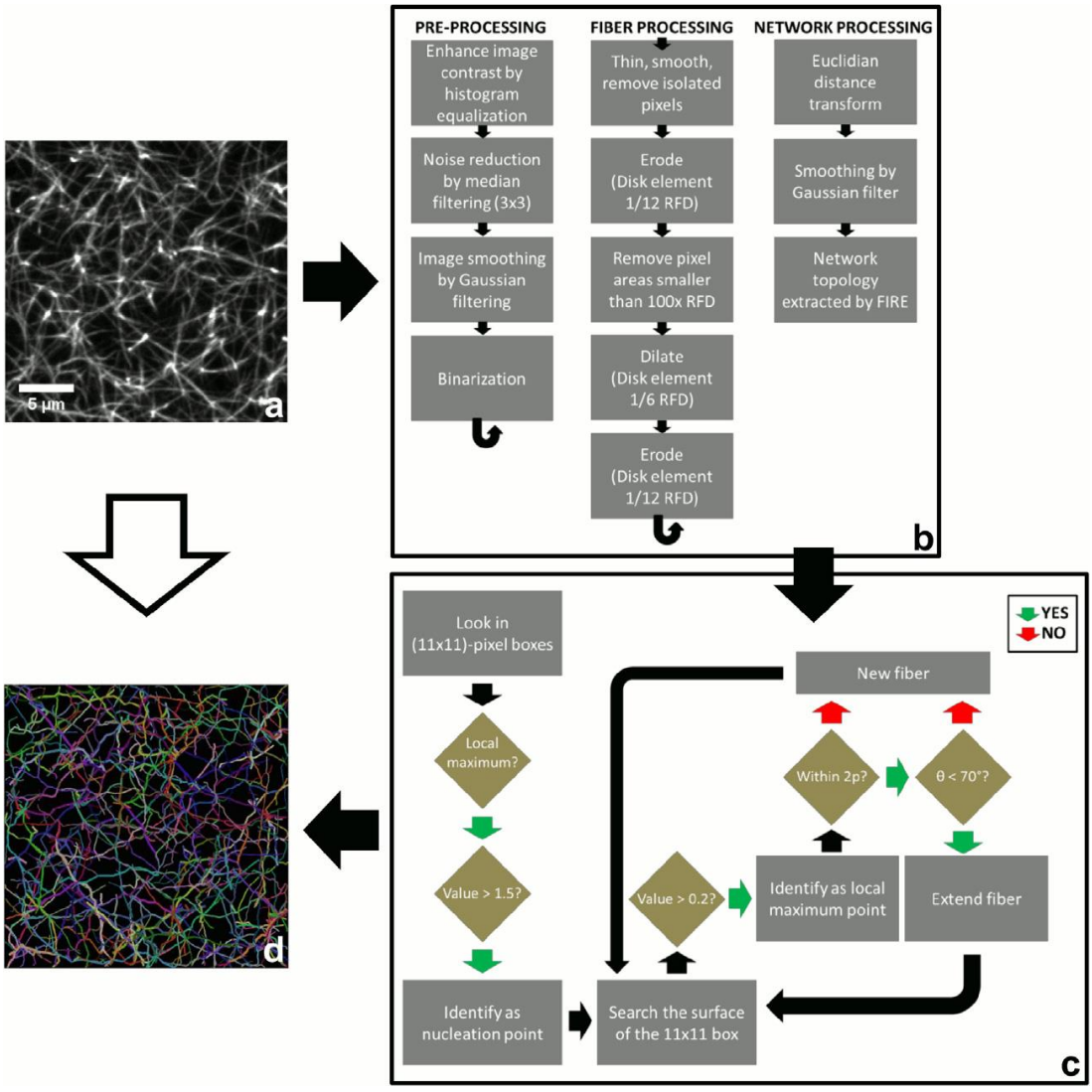

Figure 7. Outline of algorithm. (A) Original image to be processed (B) Processing steps (C) Optimization for accurate depiction of network (D) Colors for representative fibers (reprinted with permission from Elsevier) [12].

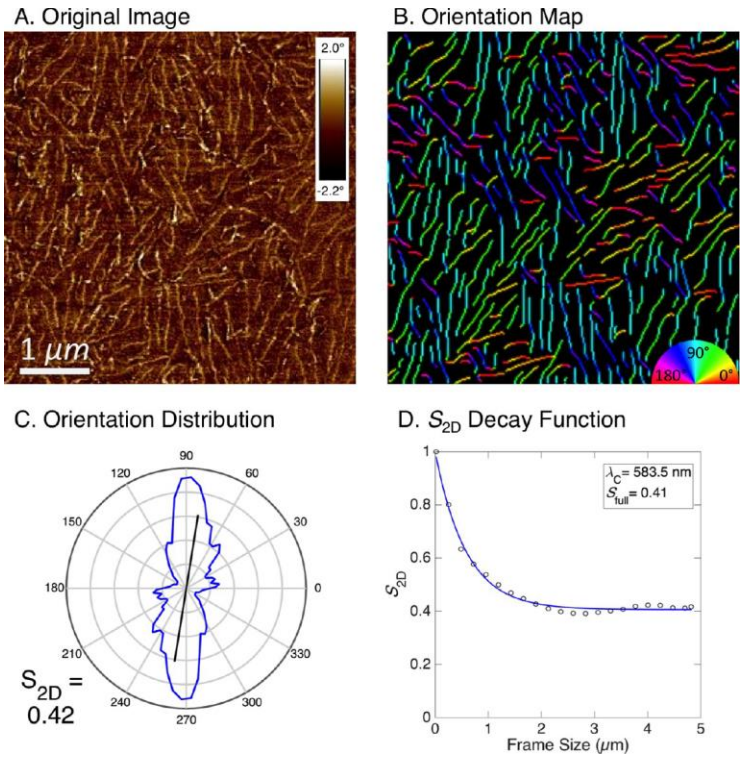

Figure 8. Results from using GTFiber. (A) Original AFM image (B) Resultant orientation map (C) Orientation distribution (D) S_{2D} plot (Reprinted (adapted) with permission from ([25]). Copyright (2017) American Chemical Society).

Another script for determining fiber network characteristics is called FiberApp which was developed by Usov et al. [26]. FiberApp uses a semi-automated process analyze fiber networks to determine several parameters, such as length distribution, orientation distribution, curvature distribution, and kink angle distribution (Figure 9). The fibers are defined manually by tracing and fitting lines over the fibers in the image. The application also allows for the generation of a fiber network with known properties, which can be used for validation of other algorithms.

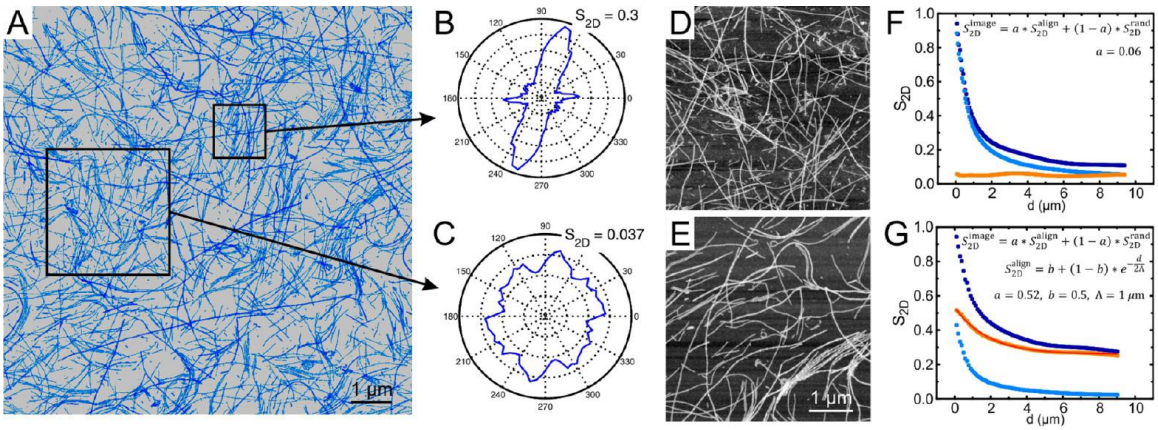

Figure 9. (A) AFM image used analyzed for orientation distribution (B, C) Orientation distribution of respective highlighted segments (D, E) AFM images analyzed for S2D decomposition (F, G) Respective S2D decomposition [26].

DiameterJ is a plugin for ImageJ that offers segmentation and fiber network analysis [27]. DiameterJ was developed to analyze nanofiber morphology where the fiber diameter, orientation, and pore size has been correlated the structural and mechanical properties [28]. The tool was validated against manual measurements by analyzing synthetically created networks of known diameters and networks of steel wires with known diameters. Fiber diameter, percent porosity, mean pore size, intersection density, and orientation distribution are some of the outputs that DiameterJ is able to determine from an SEM image of fibrous material.

2.4 Summary

The ability to quantify collagen in tissue samples was demonstrated by Minion et al. but the drawback of this method is the inability to determine localized collagen concentrations between layers. It is not feasible to split the layers to be run through an amino acid analyzer because of the friability of the layers. Rich et al. provided a method

to quantify collagen through the use of imaging software and show the differences in media collagen concentration and adventitia collagen concentration [17]. However, it is not specified how the adventitia and media are discriminated from one another. When observing the image from polarized light microscopy, it is very difficult to determine where the border between the layers is. Rich et al. also only considers the total amount of collagen observed from the PSR staining and gives relative amount of each color compared to the total content. According to, Lattouf et al. the apparent coloring from the PSR is not independent of the orientation of the platform and, thusly, cannot be taken as reliable information for collagen typing.

A better means of quantifying collagen would to be compare the bright-field microscopy images to the polarized microscopy images. PSR dyed AAA tissue shows a bright red which signifies high amounts of collagen. Thus, it can be determined these bright red sections are the adventitia which are primarily thick bundles of collagen [29]. Overlaying the bright-field image over the polarized image can allow for a border to be drawn to distinguish adventitia from media in the AAA.

The orientation distribution of fiber networks has been accomplished for collagen networks using different imaging techniques, with some established applications such as GTFiber and FiberApp. Both of these applications utilize FTM to analyze the orientation of the fibers, which is a widely accepted method for analyzing orientation distribution. However, these programs do not provide a methodology for segmentation of the images and require manual pre-processing and measuring to obtain meaningful data. Some

challenges still exist with analyzing confocal microscopy images due to the inability to properly define the edges of the fibers [23]. Also, images from confocal microscopy 2D representations of a 3D structure. It is not appropriate to treat all materials as planar so a method to determine the characteristics in 3D may be needed. Although FTM can be generalized for three dimensional structures, there is very little understanding about how the resolution in the z-stack affects the amount of measurement error [20]. Although these methods supply a distribution of the fiber orientations, these methods do not provide a means of representing the trends within the orientations of the fibers that are easily interpretable.

3.0 RESEARCH OBJECTIVE

3.1 Objective Statement

The objective of this study is to develop an automated image processing algorithm to be used to characterize fibrous biological networks. There are two major milestones for the progression of this study. First, the analysis of the collagen content was conducted using images of AAA histological sections dyed with PSR. Each section has a complementary pair of images, one from bright-field microscopy and another from polarized light microscopy. The deliverable for this effort is an automated algorithm that may be employed on any pair of PSR-stained images of aortic sections to extract collagen content in media and adventitia. Second, this study adapted and modified a DiameterJ-based algorithm to analyze the morphometric properties of blood clots. The clots were either prepared from fresh or stored platelets, and the resulting fibrin network was visualized by scanning electron microscopy (SEM). This analysis was used to correlate structural changes to the mechanical properties of blood clots.

CHAPTER FOUR: MATERIALS AND METHODS

4.1 Automated Analysis of Collagen content using MATLAB

Various imaging software, such as Adobe Photoshop, ImageJ, and MATLAB, are utilized in this thesis to visually quantify the collagen content of AAAs. The quantities are determined by analyzing images of histological samples treated with picrosirius red (PSR) under bright-field and polarized light microscopy. The colors of the collagen under polarized light will determine the overall quantity of collagen in each histological slice. The bright-field images will be used to distinguish the adventitia from the media and the polarized light images will be used to determine the overall concentration of collagen as well as the collagen in the media. Once the media has been isolated for analysis, the fiber network will be analyzed using MATLAB to determine the orientation of the fibers with respect to the axial direction of the wall.

The program for automated collagen quantification can be found at https://git.io/vhsGV. The repository must to be downloaded and extracted into the active MATLAB (2017b, Math Works) directory. The program was run within MATLAB by using the command "Automatic_Collagen_Quant_AAA_PSR." The program provided a graphical user interface (GUI) that was available to quantify the collagen using bright-field and polarized images. The following steps detail the methods that the program uses to quantify the collagen.

4.1.1 Uploading the Images

The bright-field and polarized images were uploaded into MATLAB. The images should ideally be uncompressed. TIF images are preferable to best preserve the quality of the images, although the program does allow for the uploading of other image format types.

4.1.2 Pre-Processing of Images

The uploaded images are adjusted to an array of m x n x 3 to account for images that may be in RGBa space, which outputs images in a m x n x 4 array. The third dimension of the array corresponds to the red, green, and blue intensity values, respectively. The green channel of the bright-field image was isolated by selecting the second of the three layers of the image array which resulted in a grayscale image. The polarized image was converted into grayscale using the function *rgb2gray* in MATLAB, and the contrast was improved using MATLAB's *adapthisteq* function.

4.1.3 Processing the Bright-Field Image

The grayscale image obtained from the green channel of the image was then adaptively binarized using the *imbinarize* function with a sensitivity of 0.3. This sensitivity was chosen to sufficiently thin the portions associated with the media that would later be removed through erosion and dilation techniques, and to preserve the integrity of the adventitia. Two structural elements in the form of a disk were created with diameters of four and two. The two-pixel structural element was used for erosion and the four-pixel structural element was used for dilation. The binarized image was

eroded, dilated, and eroded to remove the small fibers associated with the media, while preserving the integrity of the image. The *bwareaopen* function was used to remove objects smaller than 600 pixels, and to remove any possible residual debris. The adventitia is now isolated with an empty center which will be used as the region of interest (ROI). The ROI was calculated by finding the center of the image and using the *grayconnected* function to select all of the pixels within the borders of the adventitia. A mask was created by duplicating the ROI and scaling it to 80% of its original size. This mask was used to delete any extraneous debris in ROI.

4.1.4 Processing the Polarized Image

The polarized image, now in grayscale, was binarized using Otsu's method by using *imbinarize* with global thresholding that is separate to the threshold used on the bright-field image. The ROI was then used to isolate the collagen associated with the media, and the extra debris in the middle that may appear during binarization was removed using the mask.

4.1.5 Quantifying Collagen

The total amount of collagen was quantified by counting the number of white pixels in the binarized polarized image. The white pixels that were within the ROI were counted as collagen within the media. These values were then used to determine the percent of collagen locally. If the scale bar measurements are available, the size of the scale bar and the actual length of the scale bar may be used in their respective fields in the GUI, allowing the program to compute the surface area covered by collagen.

4.1.6 Manual Analysis of Collagen Content using Adobe Photoshop

Two operators were trained to trace the outlines between adventitia and media in the image slices. The operators were given the same set of fifteen images and manually drew a line to represent the border between the adventitia and media in the polarized light images. The outlines were drawn in Adobe Photoshop by creating a layer over the image and drawing an outline around the inside of the heavily red portions of the image, representing the border between adventitia and media. The operators were also timed to determine the amount of time that was required to trace the outlines. These outlines were then used to produce ROIs that were imported into MATLAB for collagen quantification using the same methods as previously described. The localized percentage of collagen within the automatically generated ROI and manually created ROI were then compared on scatter plot to determine if the two measurements were comparable.

4.1.7 Processing of Non-Ideal Cases

Some histological sections cannot be run through the program due to the integrity of the AAA not being properly preserved during handling. This is caused by broken rings and excessive debris within the histological section that can lead to an inaccurate assessment of the collagen content. The bright-field and polarized image could also be misaligned, which can lead to an offset of the ROI. If these images were processed as is, neither total collagen content nor regional distribution could be accurately obtained. The non-ideal cases result in an abnormal outline of the adventitia and media within the output window of the program. However, some cases may be salvaged with simple

modifications in Adobe Photoshop, although there are cases that may not be salvaged, as seen in Figure 10D.

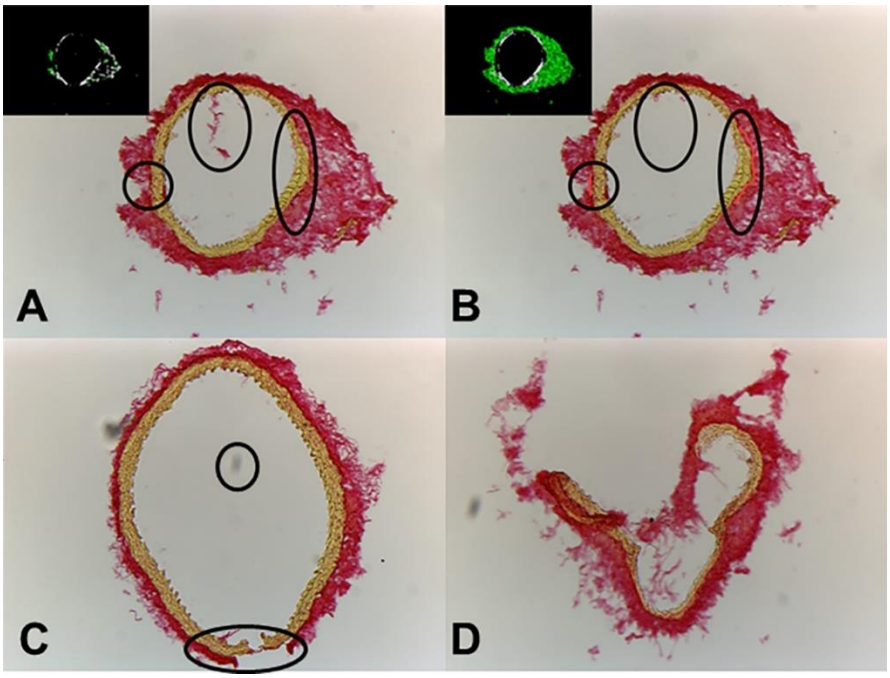

Figure 10. Sample images that require pre-processing. (A) A non-ideal image with small separations within the adventitia and excess debris and the program is not able to establish a proper ROI; (B) The non-ideal case with the excess debris removed and the adventitia bridged to produce a proper ROI for collagen quantification; (C) Another non-ideal image with corrections; (D) A non-salvageable image.

4.1.7 Statistics

We obtained 20 image sets obtained from various parts of the mouse aorta and were analyzed for total collagen content by either automated program or manually. Two operators manually traced the border between the adventitia and media for the image sets to create manually defined ROIs. These manually defined ROIs were imported into MATLAB and used to quantify the collagen by utilizing the methods used in the

program. The datasets were plotted against each other, and linear regression (GraphPad Prism) was used to compare the quality of the fit.

4.2 Characterization of Fibrin Network

SEM images (1280 x 960 pixels) of blood clots were obtained for fibrin network characterization from Nair et al. [14]. The study analyzed the morphometric characteristics of these images semi-automatically and were used to create a relationship between these characteristics and the platelet storage conditions. Automated image analysis was done on the images of fibrin clots using a combination of methods described by Hotaling et al. and Taylor et al [23, 27]. The data from the automated image analysis was then compared to the findings from Nair et al. to further establish a connection between the morphometric characteristics and the storage conditions.

4.2.1 Image Pre-Processing

The title bars of the SEM images were automatically cropped to isolate the fibrin network, which resulted in the resolution of the images being changed to 1280 x 880 pixels. The SEM images were segmented using DiameterJ's segmentation algorithm using a mix of the statistical region algorithm and traditional segmentation methods to obtain a binary image that is more easily analyzed [19, 28]. These segmented images were then used for morphometric characterization.

To prepare for the determination of the orientation of the fibers, the segmented images were skeletonized in ImageJ by inverting the binary image and using the "Skeletonize" tool, found within the menu bar under "Process > Binary > Skeletonize".

The skeletonized images were opened within Adobe Photoshop and prepared for FFT analysis using previously described methods [30]. In short, the image of the skeletonized network was inverted and a circular element with a feather mask was cropped from the image. The circular disc was rotated by 45° clockwise to prevent skewing of the data from artifacts along the cardinal directions (0°, 90°, 180°, and 270°). Figure 11 shows the outline of the process of creating the circular disk.

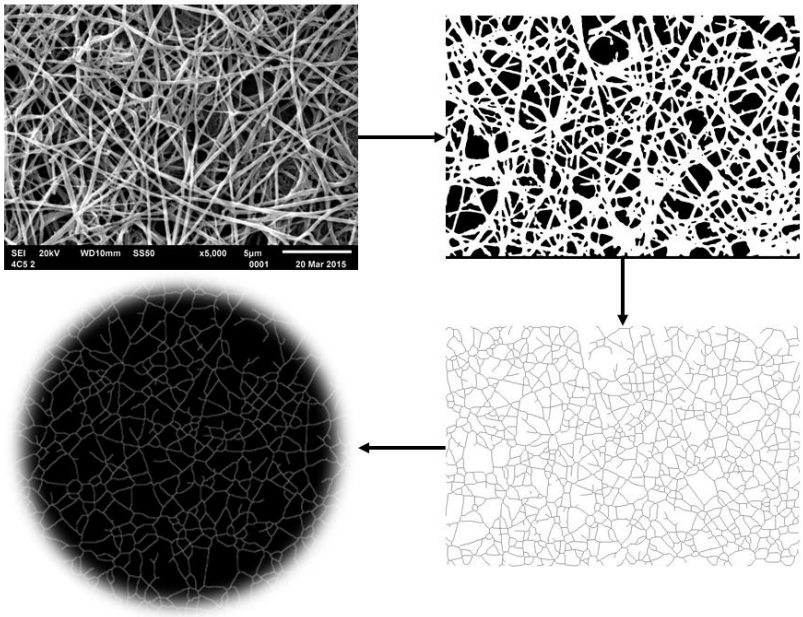

Figure 11. Process outline for obtaining circular disk for determining orientation index.

4.2.2 Morphometric Characterization

The segmented images were processed using DiameterJ to examine the morphometric properties of the fibrin networks, such as mean fiber diameter, fiber density, distribution of fiber diameters, and porosity. The mean fiber diameter was essentially determined by taking the fiber area of the branches and dividing it by the length of the centerline, which

would give the average value of the width of the fibers. Fiber density was defined as the amount of intersections that occurred per 100-pixel by 100-pixel segment of the image. Pore size and porosity of the image were calculated via built in analysis tools within ImageJ that were then incorporated into DiameterJ. The pores were defined as enclosed sections of the image that were not fibers and not enclosed by the edge of the image. The distribution of fiber diameters was represented as a histogram of fiber diameters at each point along the skeleton of the network. Plots of the morphometric processes were created for each donor to observe the characteristics of the clots.

4.2.3 Orientation Indexing

The circular element obtained from pre-processing was opened with ImageJ and the FFT of the image was generated by clicking "Process > FFT > FFT" within the menu bar. The FFT was analyzed using the plug-in, Oval Profile, which was found in the ImageJ repository at https://imagej.nih.gov/ij/plugins/oval-profile.html. A symmetrical circle selection was created on top of the FFT by selecting "Process > FFT > Make Circular Selection …". This allowed for the creating of a symmetrical and centered circle of a defined radius. This study used a 400-pixel radius to analyze the "bloom" of the FFT without including extraneous signals from the edge of the FFT. The Oval Profile plug-in was then used by clicking on "Plugins > Oval Profile" in the toolbar with "Number of Points" set to 360, the "Analysis mode" set to "Radial Sums", and the option of "Show Hotspots" unchecked. These points were chosen to analyze the intensity along each of the 360 angles of the circular selection.

The orientation data can be obtained from the Oval Profile graph by clicking “List” and plotting the values in Microsoft Excel on an x-y scatter plot. The points associated with the cardinal direction were removed from the data set, along with the points directly adjacent to the points (e.g. 90 ± 1, 180 ± 1, etc.). The orientation index was determined by processing these points in a method described by Taylor et al. [30]. To state the method briefly, values associated with the angle of interest and its orthogonal angle, along with the angles’ respective opposite angles, were normalized by dividing by the root mean square of the radial sum intensities. The normalized values of the direction of interest and its opposite angle were compared to the orthogonal direction and its opposite angle to establish a ratio of alignment along the angle of interest. The angle of interest used in this study was set at 135°, due to the rotation of the image done in the pre-processing steps.

4.2.4 Statistical Analysis

All graphs and statistical analysis were done using GraphPad Prism. Nonparametric unpaired t-tests were to determine whether the differences in the data were statistically significant with $\alpha = 0.05$. All quantifiable data were represented in graphs consisting of the mean ± the standard deviation.

CHAPTER FIVE: RESULTS AND DISCUSSION

5.1 Collagen Quantification Results

The GUI was successfully created to expedite the processing of the images. The process flow that is utilized by the program and its GUI can be seen in Figure 12 and Figure 13, respectively. As previously mentioned, each PSR-stained section has two images, each obtained from bright-field and polarized light microscopy. The program deconvolves these two images to demarcate the media and adventitia, identify the inner and outer boundaries of the two regions, and, from the residual intensities, calculate the collagen content in these regions. The green channel of the bright-field image provided the greatest amount of contrast between the media and adventitia, as can be seen in Figure 14, which allowed for the definition of the ROI.

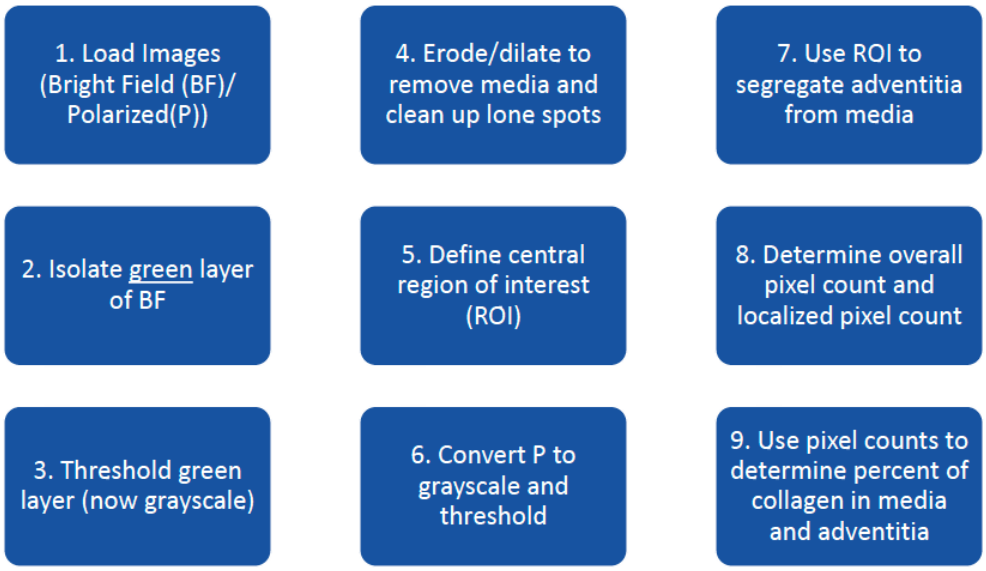

Figure 12. A simplified flowchart outlining the steps taken by the program to quantify collagen within the AAA sections.

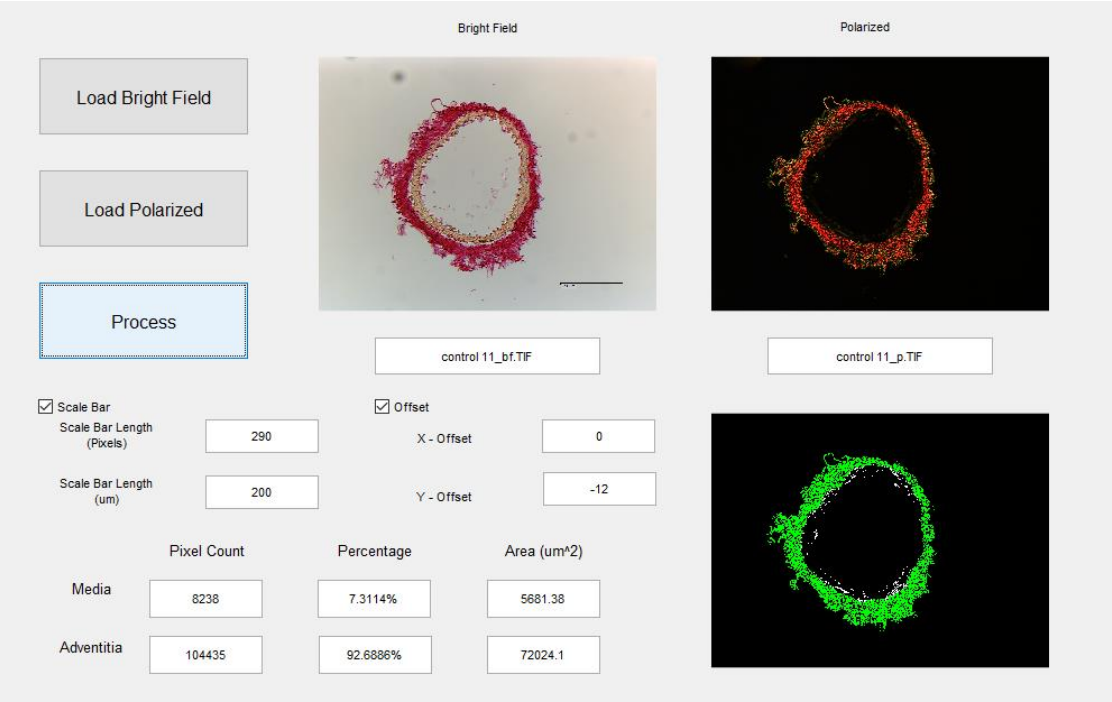

Figure 13. The GUI used by the program to quantify collagen within the adventitia and media.

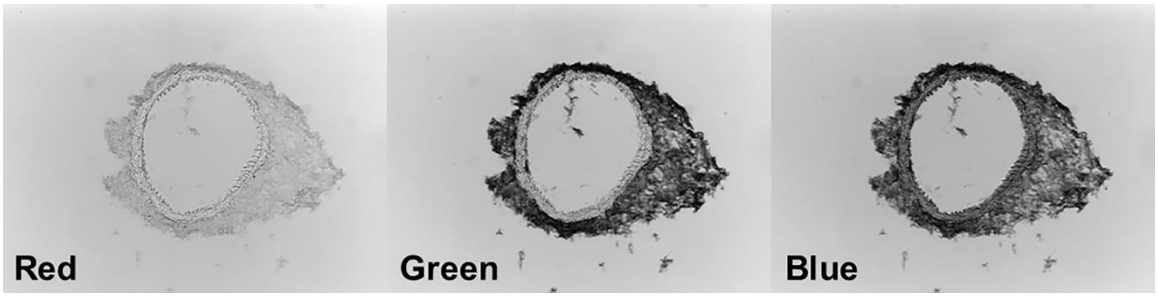

Figure 14. The RGB channels of a bright-field image.

A visual summary of the processing performed by the program can be seen in Figure 15. The bright-field images of the PSR-stained AAA sections show a distinct deep red outer ring and an orange-yellow inner ring (Figure 15A). The outer red stain is representative of the adventitia due to the large amount of collagen bundling within that

layer of the vessel wall. The orange-yellow ring is representative of the media and, although it is not immediately apparently under bright-field, there is collagen that is present within this portion of the vessel wall. Polarized light microscopy allows for the observation of the collagen that is present within the media (Figure 15D). Therefore, polarized light microscopy in combination with PSR is most useful when used for the visual quantification of the overall collagen content since the colors are easily differentiated from the black background.

The program operates on the assumption that the histological section has a continuous adventitia and there is minimal debris on the slide. It also operates on the assumption that the ROI is in the center of the image and that the bright-field and polarized light microscopy images are perfectly aligned. In this study, it was observed that many samples were not ideal samples for automatic quantification. If these samples were processed as is with the program, no meaningful data would be obtained. Fortunately, some non-ideal cases can be processed by the program after some modification using Adobe Photoshop.

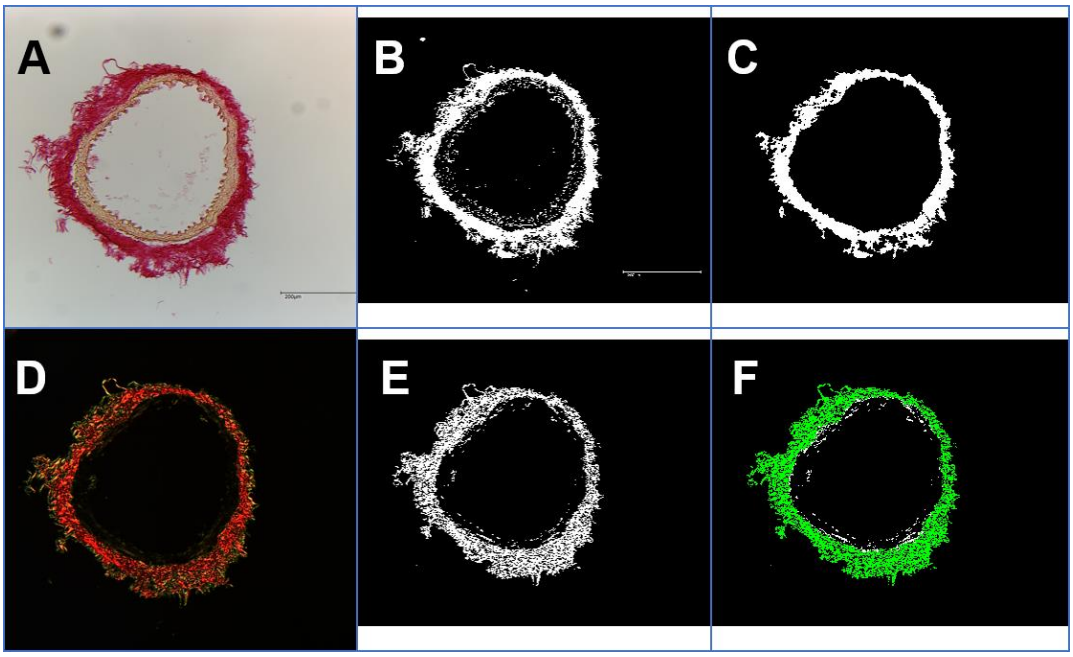

Figure 15. The original bright-field (A) and polarized light microscopy images (D); Segmented portions after conversions to grayscale from the bright-field image (B), and from the polarized image (E). The segmented images from (B) were subjected to a cycle of erosion, dilation, and erosion to remove the pixel associated with the media while maintaining image integrity (C). Isolated islands were also removed to remove extraneous debris. A visual representation of the polarized image separated by adventitia (green) and the media (white) (F).

The following steps were taken to pre-process the images for the program in the event of non-ideal image:

(i) Broken adventitia: The adventitia can be bridged to make it continuous using Adobe Photoshop. The eyedropper tool was used to sample the color of the adventitia. Using the pencil tool with the width set at 8 pixels, any gaps throughout the adventitia were bridged, without overlapping the media.

(ii) Excessive debris: The clone stamp was used tool to mask the debris and preserve the integrity of the image, as to not negatively affect future segmentation.

(iii) Misaligned bright-field and polarized images: This study observed a consistent 12-pixel vertical offset between the bright-field and polarized images, probably due to physical reasons while switching the filters in the microscope. To nullify this offset, the value of the offset was obtained by manual aligning of one set of images. This value was entered in the GUI before processing by clicking the check box next to “Offset” in the GUI and feeding in the x and y offsets in their respective fields.

5.2 Collagen Quantification Validation

When comparing the two operators, the average required amount of time to define the ROI was four minutes per image. On the other hand, the program can process the images, define the ROI, and quantify the collagen in a matter of seconds, and allows for a consistency of measurement between samples. The results were virtually identical between the automated method and the manual measurements, which can be seen in Figure 16A, where the relationship is almost linear, with an R-squared value of 0.94. At higher media collagen content, the manual methods consistently over-measured the amount of collagen within the media. The reason is that the automated algorithm can work inherently more easily on a pixel-by-pixel basis when compared to a human, and this difference is exemplified in Figure 16B. Since the ROI is being defined by the stark

contrast between the coloration in the layers, it is highly dependent on the ability to distinguish between the layers. When doing manual analysis, any number of factors can lead to inaccuracies such as the steadiness or fatigue of the hand, the accuracy/resolution of the mouse/trackpad itself, and the amount of time necessary to achieve the same kind of outline that is supplied by the program. In contrast, since the automated algorithm operates on a rigid set of rules, it is an ideal method for consistent demarcation between layers. For instance, in Figure 16B, the number of pixels for the segment shown was determined to be 15,406 pixels out of the 219,375 pixels of the entire sample. The errors made using the manual method lead to an over-measurement of 565 pixels, shown in green.

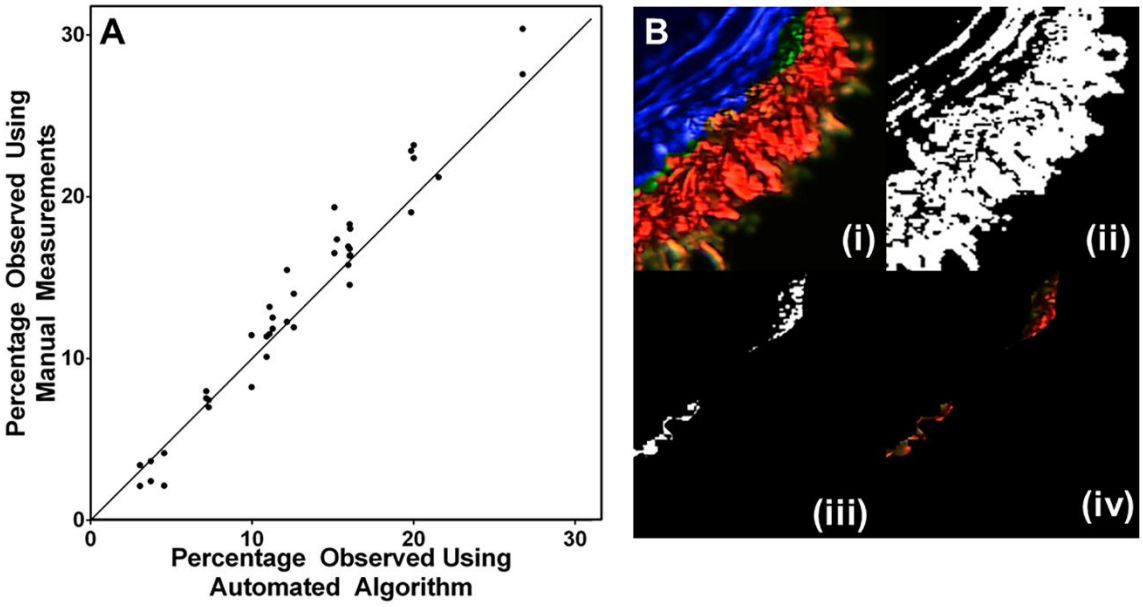

Figure 16. (A) Scatter plot demonstrating the similarity between manually defining the ROI and automatically defining the ROI with the program (n = 20). The methods produced virtually identical results at lower collagen levels although the manual method overpredicted at higher collagen levels (R2 = 0.94). (B) Accuracy of the automatic program vs. manual tracing. (i) A subsection of a polarized image with the ROI generated by the automated program (blue) and by manual tracing (green); (ii) Binarized image; (iii) The extra pixels that were counted after global thresholding in manual measurement but not automated algorithm; (iv) The extra pixels were pixels that should be attributed to adventitia by showing the pixels were associated with red color.

5.3 Morphometric Characterization of the Fibrin Network

Nair et al. used semi-automated processes to quantify the architecture of clots. Some of the parameters that were measured were fiber density, fiber length, and the distribution of fiber diameters. The methods used in this study were used to automatically quantify these parameters, as well as analyze the porosity of the clots and provide data on the orientation distribution of the fibers. The morphometric properties of clots formed from

fresh plasma were mainly used to compare the methods between Nair et al. and this study.

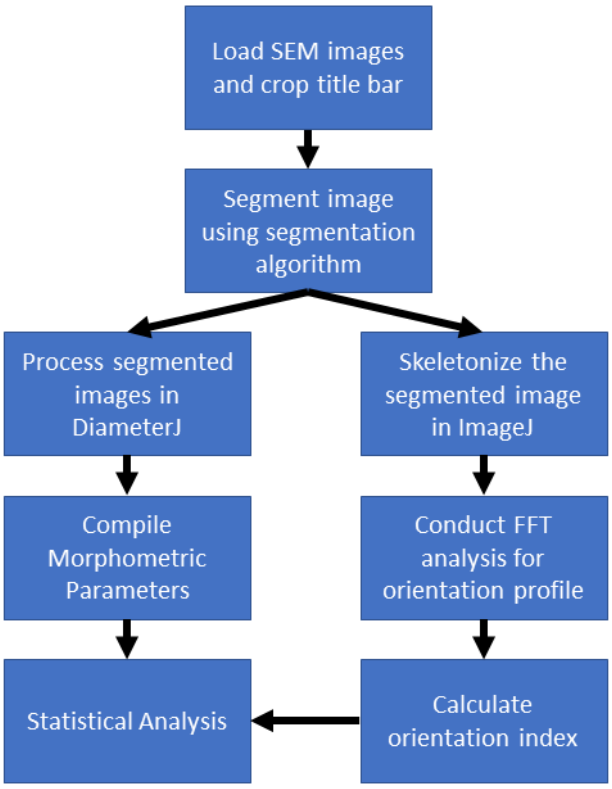

Figure 17. A simplified flowchart of the methods for processing the SEM images for morphometric analysis and orientation indexing.

The distribution of fiber diameters was previously determined by using a combination of ImageJ and MATLAB programs to threshold the image and 100-pixel by 100-pixel grid lines were applied to the image. A combination of edge detection techniques and gray-scale gradient calculations were then used to find the distribution of fiber diameters. DiameterJ offered two different methods for characterization of the fiber diameter. One method is described as the “Super Pixel” value which is essentially the mean fiber

diameter. This was achieved by creating a skeleton of the image and using the centerlines of the skeleton in combination with the white pixels associated with the fibers to reach a value for mean fiber diameter. The second method is similar to those used in the previous, in which a histogram of fiber diameters was created to describe the distribution of fibers of different diameters. Nair et al. determined that the fibers had a large distribution of fibers at approximately 200 nm [14]. However, the automated program showed a higher distribution of smaller fibers, with a peak at 100 nm (Figure 18). This is most likely attributed to the segmentation method used in this study, due to the segmentation algorithm including more of the smaller fibers that could be omitted as background in the previous study. The previous study could also have some skewed results due to the change of aspect ratio of the original image. The original images are in a 4:3 aspect ratio, but the previous study had to transform the images into a square (1:1) ratio image in order to create the 100-pixel by 100-pixel grid.

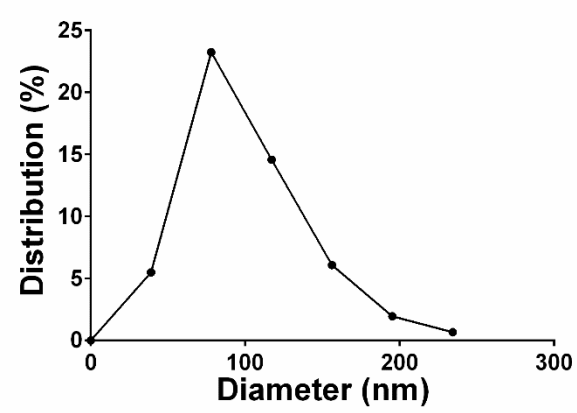

Figure 18. Distribution of fiber diameters throughout the SEM images of clots from fresh plasma.

Fiber density of the network was determined in the previous study by creating short sequences across the image that were approximately one third of the width of the image. The fiber density was determined by manually counting the number of times the fibers crossed across these sequences. As mentioned previously, the automatic determination of fiber density was represented by an average of intersections per square micron. The quantification was performed by identifying the total amount of intersections and dividing that number by the area of the image, which was then multiplied by 100 pixels by 100 pixels (10^4). This value was then converted into square microns using the values given by the scale bar of the image. The intersection densities of the fibrin network are represented in Figure 19B, where the intersection density varied between 2.6 and 4.7 intersections/μm^2. The automated quantification offered a more intuitive interpretation of the fiber density than that of the previous by offering the amount of intersections per surface area, which is more representative of the entire network.

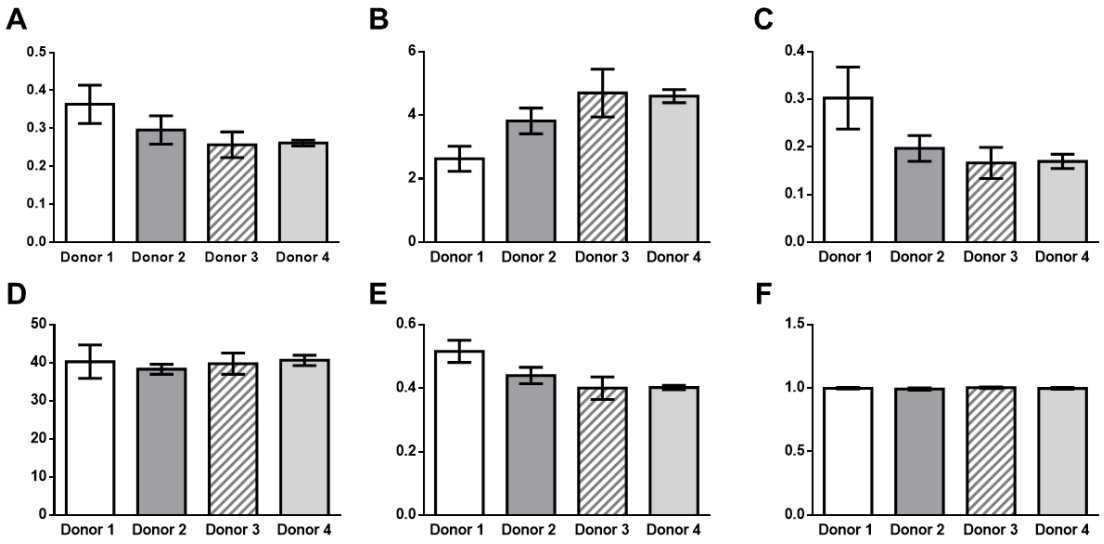

Figure 19. Morphometric properties of fibrin networks formed from fresh plasma. (A) Mean fiber diameter (μm) (B) Fiber density (intersections/μm^2) (C) Mean pore area (μm^2) (D) Porosity (%) (E) Characteristic fiber length (μm) (F) Orientation index.

The characteristic fiber length was determined by taking the average of fiber lengths between branching points. The previous study manually traced between branching points to determine the length of the fibers. As seen in Figure 19E, the automated characterization determined that the characteristic fiber length was around 0.5 μm, but the values were seen to be around 5 μm when measured manually. This large discrepancy is due to the inclusion of the background fibers from the segmentation algorithm. As fibers overlap, the program is unable to discern that overlap from a branching point, thus undercalculating the length of the fiber. In order to properly characterize the length of the fibers in the SEM, additional manual alterations must be performed to remove the

backing fibers, but the program is unable to distinguish between branches and overlaps in its current state.

The porosity of clots was comparable between all the samples, but the mean pore sizes varied between the donors (Figure 19C and Figure 19D). The fiber density also changed inversely to the mean pore area, which is expected as there are larger voids, there are less bundles of fibers within the fibrin network. The mean fiber diameter also had a slight trend with mean pore area, which would suggest that, although the network was less dense, the fibers were thicker in the samples with larger pores. Combining these changes between donors can account for the unchanged porosity between samples.

Images of clots formed from plasma that was stored at room temperature were also analyzed to determine the morphometric properties of the fibrin network. The architecture of the clots formed from stored plasma and fresh plasma were compared in an attempt to draw a relationship between the morphology and the mechanical response found in the previous study (Figure 20). The previous study stated that fresh plasma formed more superior clots than stored plasma, with respect to their respective mechanical properties. The mean fiber diameter, mean pore area, and characteristic length of the networks obtained from the stored clots were higher than the fresh clots. Although the stored clots are supposed to be weaker, the fibers were shown to have increased fiber diameter, which would suggest that stored plasma produced a stronger clot due to thicker fibers. However, it has already been demonstrated that the fresh

plasma produces a superior clot, which leads to the suggestion that fiber diameter may not be a principle parameter in determining clot strength.

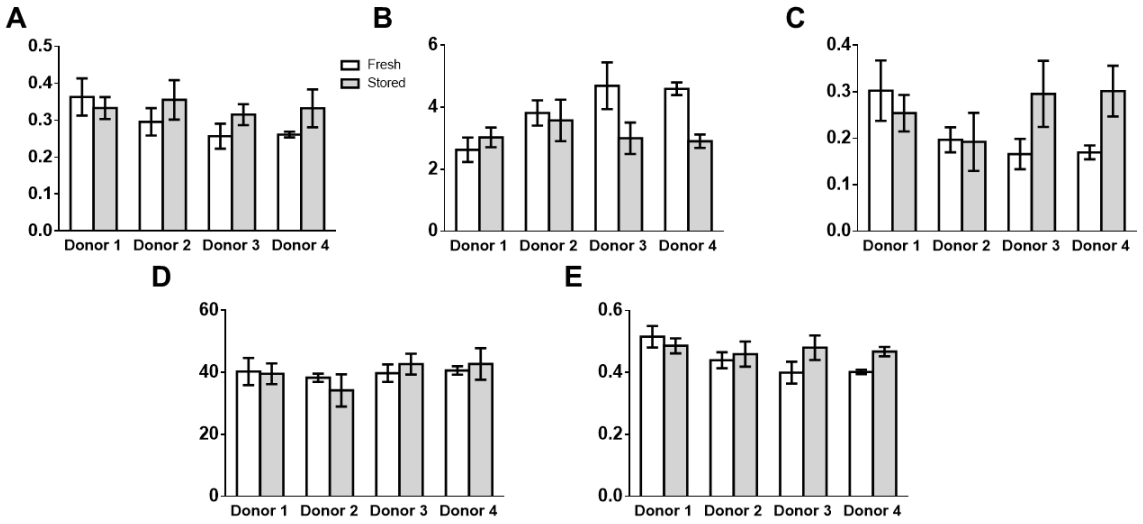

Figure 20. Comparison of the morphometric properties of clots formed from fresh plasma and stored plasma. (A) Mean fiber diameter (μm) (B) Fiber density (intersections/μm^2) (C) Mean pore area (μm^2) (D) Porosity (%) and (E) Characteristic fiber length (μm).

The stored clot morphology also produced an inverse relationship between fiber density and mean pore area that was observed with the fresh clots. The clots from fresh plasma produced clots with higher fiber density and the clots formed from stored plasma tended to have a higher mean pore area. The combination of this data alludes to the density of the fiber network being a primary contributor to the strength of the clot. Since the fibrin network of the stored clot was determined to be sparse, there was a greater variation in porosity than what was seen in the fresh clots. This was likely due to the lack of background fibers in the SEM images of the fibrin network.

The sparsity of the fibers and the lack of background clots also had an effect of the characteristic fiber length. Since less background fibers existed within the stored clots, the errors that could have been due to the misrepresentation of fiber overlaps as branches could also have been reduced.

Statistical analysis of the means of the morphometric parameters between the fibrin networks formed from fresh and stored plasma was performed. Figure 21 shows a comparison of the averages of the characteristics of the two clot types. It was determined that each parameter was significantly significant, except for the orientation index and the porosity. Even though the changes in the porosity were not considered to be statistically significant, there is significance in the overall porosity remaining unchanged in spite of the mean pore areas changing, as previously mentioned.

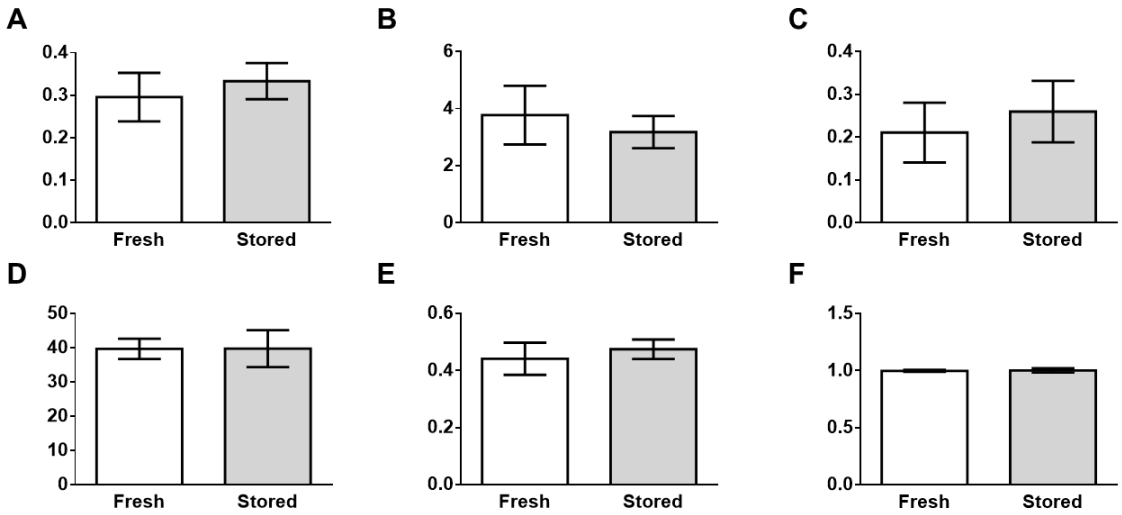

Figure 21. A comparison between the averages of the morphometric values of the fresh and stored clots. (A) Mean fiber diameter (μm) (B) Fiber density (intersections/μm^2) (C) Mean pore area (μm^2) (D) Porosity (%) (E) Characteristic fiber length (μm^2) and (F) Orientation index.

5.4 Orientation Index

The mechanical properties of the clot can also be largely determined by the architecture of the fibrin, which also includes the arrangement of these fibers. Although DiameterJ offered orientation data, the data was difficult to interpret and quantify. Thus, the method of establishing a comparison of a direction of interest in relation to its orthogonal direction used by Taylor et al. was used. An orientation index of 1.0 can be seen as an image that is evenly oriented between the direction of interest and its orthogonal direction. Values larger value than 1.0 meant that the fibers were oriented in the direction of interest and values smaller than 1.0 meant that the fibers were oriented more towards the orthogonal direction. The average orientation indices of the donors can be seen in Figure 19F, where there is no discernible difference between the donors. Since the values were all approximately 1.0, it was determined that the fibers were evenly distributed in both directions.

To test extreme cases using this method of determining an orientation index, an image of a black circle with a single one-pixel line going across at a 45° angle was generated and analyzed to determine its orientation index. The RMS of the data becomes somewhat skewed due to the signal generated by the line not being strong enough to neglect the axial signals from the FFT. However, very strong peaks can be seen at the angles of interest and virtually no signal is found at the orthogonal angles. This image resulted in an orientation index of 1.229, even with the significantly weaker signals at the orthogonal

angle. The index could increase if the signal was increased by including fibers or by thickening the fiber. This implies that although the image seems to have a small change in orientation index, it could be indicative of a larger change.

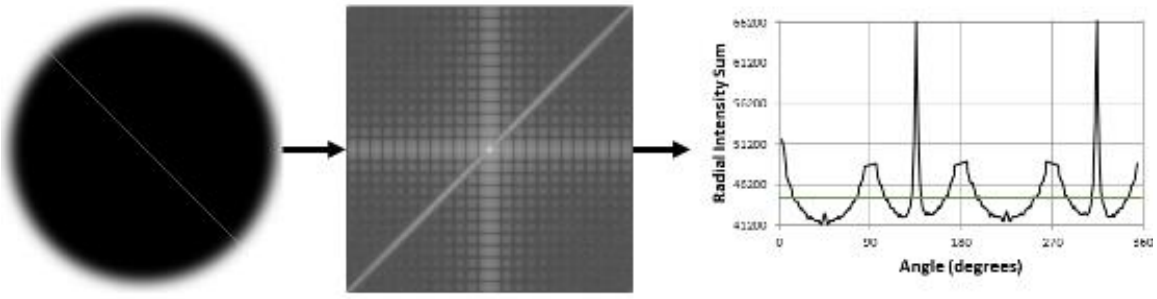

Figure 22. Determining the orientation index of a singular one-pixel white line on a black background.

The orientation index of clots formed from room-temperature stored plasma was also determined were compared to each other in Figure 23. The orientation indices also were approximately 1.0, although there was a very slight increase in alignment along the direction of interest for the clots from stored plasma. The maximum and minimum orientation indices for the room-temperature clots were 1.1013 and 0.977 respectively. The maximum and minimum of the fresh clots were 1.021 and 0.975. As seen in the previous figure, although the orientation index was only slightly higher in the stored plasma, it could have a larger implication on the ultrastructure of the clot. However, this slight change was determined to be statistically insignificant, with a P value of 0.68.

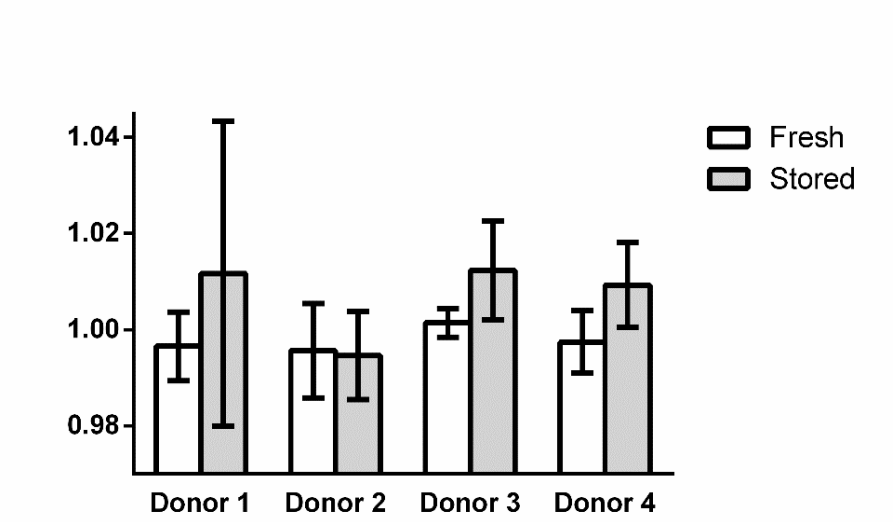

Figure 23. Comparison of average orientation indices of the fibrin networks resulting from stored and fresh plasma.

CHAPTER SIX: CONCLUSIONS & FUTURE WORK

The characterization of collagen and fibrin within soft tissue networks is important for understanding the mechanical behavior blood vessels and blood clots in both physiology and pathophysiology. The development of automated image analysis allows for rapid characterization of fibrous networks in tissue. This study provides two different methods to analyze certain soft tissue via images obtained through SEM, polarized light microscopy, and bright-field microscopy. The local quantification of collagen within AAA sections was successfully executed and offered a quicker and more accurate measurement than what could be done manually. The high contrast of the bright-field image allowed for the differentiation of the media from the adventitia via color layer separation. This allowed for a perfectly sized stencil of the area that occupies the media that was utilized to then distinguish between adventitia and media in the image obtained by polarized light microscopy. The program also utilizes a simple and intuitive GUI that allows for the operation of the program with little to no training.

The ultrastructure of the fibrin network of clots was visually characterized with varying success. The program determined the mean fiber diameter, fiber density, mean pore area, percent porosity, and characteristic fiber length of fibrin in SEM images of clots. The determination of characteristic length differed greatly from what was observed in previous studies and may not be truly representative of the fiber lengths due to the program's inability to distinguish between fiber branches and fiber overlaps. Out of these morphometric parameters, it was concluded that the changes in mean fiber diameter, fiber

density, and mean pore area were the physical characteristics that may determine the mechanical response of the clot. The orientation distribution of the fibers was also characterized, and the distribution was expressed as an orientation index, which was a value that indicated the extent that the fibers favored a pre-determined direction. The orientation indices revealed that the fibers were mostly evenly distributed in the angles of interest and their respective orthogonal angles, which may prove that the seemingly random nature of the fibers could not be used to predict mechanical behavior.

Moving forward with these automated methods, there remain some challenges with the segmentation of the AAA sections, especially if the histological section has excessively uneven lighting. This study utilized an adaptive histogram equalization algorithm to bypass these issues, but some images were still too unevenly lit to achieve sufficient segmentation. Machine learning-based segmentation algorithms have been utilized by some studies and may be applied to accurately define the edges of the image obtained using polarized light microscopy.

The collagen quantification program also operates on the assumption that the AAA is going to be a complete section that is ring shaped. This circular shape can allow for automated local quantification of collagen in the radial direction. A radial distribution of collagen could prove useful when studying disease in blood vessel walls, especially if trends are found within a certain direction of the tissue.

As previously mentioned, characterizing the length of the fibrin fibers in the blood clots can be difficult to do automatically. To get accurate measurements, the fibers that

are not on the same plane as the fibers of interest would need to manually be removed. However, as mentioned with automated collagen quantification algorithm, there has been work done on using machine learning to efficiently find edges and segment the images accurately along all edges.

The orientation index proved to not yield significant data with respect to the changes caused by storage conditions. However, Nair et al. did measure the curvature of some of the fibers with the network and it was observed that the stored plasma yielded clots with fibrin that had greater curvature. The curvature was measured semi-automatically, where the fibers were manually traced and analyzed for curvature. Since DiameterJ is able to find the nodes where there is branching of fibers, there could possibly be more work done to analyze how drastically the fibers deviate from a straight line that goes from node to node.

This study presents a methodology for automatically characterizing soft tissue using image analysis software. The automatic quantification of collagen within AAA tissue allowed for rapid processing and consistent results, and the program was comparable to manual techniques. The automatic characterization of the fibrin networks was accomplished using previous described methods and these characteristics were used to relate the ultrastructure to previously studied mechanics. Although improvements could be made regarding the segmentation of the images, this study provides valuable methods for use in future studies of soft tissue and disease.

REFERENCES

[1] R. R. Minor, "*Collagen metabolism: A Comparison of Diseases of Collagen and Diseases Affecting Collagen,*" Am. J. Pathol., **98**, 225–280, (1980).

[2] J. E. Wagenseil and R. P. Mecham, "*Vascular Extracellular Matrix and Arterial Mechanics,*" Physiol. Rev., **89**, 957–989, (2009).

[3] N. Sakalihasan, R. Limet, and O. Defawe, "*Abdominal aortic aneurysm,*" Lancet, **365**, 1577–1589, (2005).

[4] C. M. He and M. R. Roach, "*The composition and mechanical properties of abdominal aortic aneurysms,*" J. Vasc. Surg., **20**, 6–13, (1994).

[5] H. Chen and G. S. Kassab, "*Microstructure-based biomechanics of coronary arteries in health and disease,*" J. Biomech., **49**, 2548–2559, (2016).

[6] J. S. Bell, A. O. Adio, A. Pitt, L. Hayman, C. E. Thorn, A. C. Shore, J. L. Whatmore, and C. P. Winlove, "*Microstructure and mechanics of human resistance arteries,*" Am. J. Physiol. - Hear. Circ. Physiol., **311**, H1560–H1568, (2016).

[7] J. Satta, T. Juvonen, K. Haukipuro, M. Juvonen, and M. I. Kairaluoma, "*Increased turnover of collagen in abdominal aortic aneurysms, demonstrated by measuring the concentration of the aminoterminal propeptide of type III procollagen in peripheral and aortal blood samples,*" J. Vasc. Surg., **22**, 155–160, (1995).

[8] C. Buckley, C. W. Wyble, M. Borhani, T. L. Ennis, D. K. Kobayashi, J. A. Curci, S. D. Shapiro, and R. W. Thompson, "*Accelerated enlargement of experimental abdominal aortic aneurysms in a mouse model of chronic cigarette smoke exposure,*" J. Am. Coll. Surg., **199**, 896–903, (2004).

[9] M. Raveendran, D. Senthil, B. Utama, Y. Shen, D. Dudley, J. Wang, Y. Zhang, and X. L. Wang, "*Cigarette suppresses the expression of P4Hα and vascular collagen production,*" Biochem. Biophys. Res. Commun., **323**, 592–598, (2004).

[10] J. W. Weisel, "*The mechanical properties of fibrin for basic scientists and clinicians,*" Biophys. Chem., **112**, 267–276, (2004).

[11] M. De Spirito, G. Arcòvito, M. Papi, M. Rocco, and F. Ferri, "*Small- and wide-angle elastic light scattering study of fibrin structure,*" in *Journal of Applied Crystallography*, 2003.

[12] K. A. Leonidakis, P. Bhattacharya, J. Patterson, B. E. Vos, G. H. Koenderink, J. Vermant, D. Lambrechts, M. Roeffaers, and H. Van Oosterwyck, "*Fibrin structural and diffusional analysis suggests that fibers are permeable to solute transport,*" Acta Biomater., **47**, 25–39, (2017).

[13] E. A. Ryan, L. F. Mockros, J. W. Weisel, and L. Lorand, "*Structural origins of fibrin clot rheology,*" Biophys. J., (1999).

[14] P. M. Nair, S. G. Pandya, S. F. Dallo, K. M. Reddoch, R. K. Montgomery, H. F. Pidcoke, A. P. Cap, and A. K. Ramasubramanian, "*Platelets stored at 4°C contribute to superior clot properties compared to current standard-of-care through fibrin-crosslinking,*" Br. J. Haematol., **178**, 119–129, (2017).

[15] D. J. Minion, V. A. Davis, P. A. Nejezchleb, Y. Wang, B. M. McManus, and B. T. Baxter, "*Elastin is increased in abdominal aortic aneurysms.,*" *The Journal of surgical research*, **57**. 443–446, 1994.

[16] M. Carmo, L. Colombo, A. Bruno, F. R. M. Corsi, L. Roncoroni, M. S. Cuttin, F. Radice, E. Mussini, and P. G. Settembrini, "*Alteration of elastin, collagen and their cross-links in abdominal aortic aneurysms,*" Eur. J. Vasc. Endovasc. Surg., **23**, 543–549, (2002).

[17] L. Rich and P. Whittaker, "*Collagen and Picrosirius Red Staining : a Polarized Light Assessment of Fibrillar Hue and Spatial Distribution,*" Braz J Morphol Sci, **22**, 97–104, (2005).

[18] R. Lattouf, R. Younes, D. Lutomski, N. Naaman, G. Godeau, K. Senni, and S. Changotade, "*Picrosirius Red Staining: A Useful Tool to Appraise Collagen Networks in Normal and Pathological Tissues,*" J. Histochem. Cytochem., **62**, 751–758, (2014).

[19] B. Vogel, H. Siebert, and U. Hofmann, "*MethodsX Determination of collagen content within picrosirius red stained paraffin-embedded tissue sections using fluorescence microscopy,*" **2**, 124–134, (2015).

[20] E. A. Sander and V. H. Barocas, "*Comparison of 2D fiber network orientation measurement methods,*" J. Biomed. Mater. Res. - Part A, **88**, 322–331, (2009).

[21] H. Chen, Y. Liu, M. N. Slipchenko, X. Zhao, J. X. Cheng, and G. S. Kassab, "*The layered structure of coronary adventitia under mechanical load,*" Biophys. J., **101**, 2555–2562, (2011).

[22] D. Vader, A. Kabla, D. Weitz, and L. Mahadevan, "*Strain-induced alignment in collagen gels*," PLoS One, **4**, (2009).

[23] A. D'Amore, J. A. Stella, W. R. Wagner, and M. S. Sacks, "*Characterization of the complete fiber network topology of planar fibrous tissues and scaffolds*," Biomaterials, **31**, 5345–5354, (2010).

[24] N. Otsu, "*A Threshold Selection Method from Gray-Level Histograms*," IEEE Trans. Syst. Man. Cybern., **9**, 62–66, (1979).

[25] N. E. Persson, M. A. McBride, M. A. Grover, and E. Reichmanis, "*Automated analysis of orientational order in images of fibrillar materials*," Chem. Mater., **29**, 3–14, (2017).

[26] I. Usov and R. Mezzenga, "*FiberApp: An open-source software for tracking and analyzing polymers, filaments, biomacromolecules, and fibrous objects*," Macromolecules, **48**, 1269–1280, (2015).

[27] N. A. Hotaling, K. Bharti, H. Kriel, and C. G. Simon, "*DiameterJ: A validated open source nanofiber diameter measurement tool*," Biomaterials, (2015).

[28] I. Keun Kwon, S. Kidoaki, and T. Matsuda, "*Electrospun nano- to microfiber fabrics made of biodegradable copolyesters: Structural characteristics, mechanical properties and cell adhesion potential*," Biomaterials, **26**, 3929–3939, (2005).

[29] A. Tsamis, J. T. Krawiec, and D. A. Vorp, "*Elastin and collagen fibre microstructure of the human aorta in ageing and disease: a review*," J. R. Soc. Interface, **10**, 20121004–20121004, (2013).

[30] S. E. Taylor, T. Cao, P. M. Talauliker, and J. Lifshitz, "*Objective morphological quantification of microscopic images using a Fast Fourier Transform (FFT) analysis*," Curr. Protoc. Essent. Lab. Tech., (2013).

[31] R. Nock and F. Nielsen, "*Statistical region merging*," IEEE Trans. Pattern Anal. Mach. Intell., (2004).